Clays and Clay Minerals, Vol. 55, No. 4, 423–442, 2007.

METAMORPHIC-HOSTED PYROPHYLLITE AND DICKITE OCCURRENCES FROM THE HYDROUS Al-SILICATE DEPOSITS OF THE MALATYA-PÜTÜRGE REGION, CENTRAL EASTERN ANATOLIA, TURKEY

ÖMER BOZKAYA*, HÜSEYİN YALÇIN, ZEYNEL BAŞIBÜYÜK AND GÜLCAN BOZKAYA

Department of Geological Engineering, Cumhuriyet University, TR-58140, Sivas, Turkey

Abstract—Hydrous Al-silicate deposits are found to the south of Pütürge in Malatya city, Turkey. The surrounding rocks consist of mylonitic granitic gneiss overlain by muscovite gneiss with kyanite-bearing metabasic schist lenses on top which are cut by silica veins containing prismatic tourmaline and specularite. Pyrophyllite is found within kyanite gneisses overlying the granitic gneisses. Fibrous, platy pyrophyllite is developed along the edges and cleavage planes of kyanite, whereas platy bunches of dickite occur as replacements of the relict kyanites as well as crack- and pore-fillings. Rocks forming the hydrous Al-silicate deposit contain $2M_1$ pyrophyllite, alunite, topaz, paragonite, dravite, dumortierite, chlorite and epidote as early hypogene minerals, and $2M_1$ dickite, diaspore, gibbsite, specularite, goethite and crandallite/goyazite as late hypogene minerals. On the basis of fluid inclusion and stable isotope data, it is estimated alterations to pyrophyllite and kaolinite occurred at temperatures are of 150 and 100ºC, respectively, the minerals being formed by meteoric waters interacting with metamorphic rocks. Trace and *REE* variations are highly distinctive in terms of enrichment of most trace elements in pyrophyllite, whereas *REE*s are clearly abundant in dickite, indicating different conditions during formation such as early and late hypogene processes. The pyrophyllitic alteration took place in the late Cretaceous (69−71 Ma), whereas kaolinization occurred later.

Key Words—Dickite, Geochemistry, Hydrothermal Alteration, Mineralogy, Pyrophyllite.

INTRODUCTION

Pyrophyllite is a relatively uncommon mineral compared to kaolin minerals and is used as a raw material in many industrial applications, particularly in ceramics, refractory, cement and mosaics. In contrast to some materials such as talc and clays, the expansion in pyrophyllite is permanent due to water loss and the separation of phyllosilicate layers, which permits pyrophyllite to be used to manipulate the shrinkage and thermal expansion of various clay bodies (Kutbay, 1998). Nearly 80% of the 2.2 million tons of annual world pyrophyllite production comes from Japan and South Korea. The remainder is produced by Brazil, India, USA, Pakistan and Thailand. Europe's only mine working pyrophyllitic rocks is in the Pütürge region in Malatya city, Turkey. It has approximate reserves of 6−7 million tons and its production has reached up to 120,000 tons/year in recent years (Uygun and Solakoğlu, 2002).

Pyrophyllite is often associated intimately with dickite and other minerals such as muscovite, paragonite and chlorite in different geological environments. Pyrophyllite and dickite are formed mainly by the hydrothermal alteration of acidic volcanic rocks (*e.g.* Murray, 1988; Marumo, 1989; Terakado and Fujitani, 1998; Nabetani and Shikazono, 2002; Kontak *et al.*, 2004). Pyrophyllite is generated in pelitic rocks during greenschist or incipient regional metamorphism (Frey, 1987; Evans and Guggenheim, 1988; Merriman and Peacor, 1999; Bozkaya and Yalçın, 2004a, 2004b). In addition, dickite is also found as widespread authigenic and transformation components of various siliciclastic rocks having no apparent association with hydrothermal activity (Ruiz-Cruz and Reyes, 1998; Veniale *et al.*, 2002).

The Pütürge deposit has not been investigated in detail thus far. This deposit is a hydrous Al-silicate deposit (HASD) given the presence of pyrophyllite with dickite and lesser amounts of alunite, diaspore, kyanite, gibbsite and topaz. The geology of the Pütürge HASD and its vicinity has been investigated by the General Directorate of Mineral Research and Exploration (Danış, 1978; Telek, 1979; Aras and Açıkgöz, 1992; Yılmaz., 1993). In addition, as it is an area of critical regional geotectonic importance in Turkey, it was investigated by other authors (Yazgan and Chessex, 1991; Yılmaz, 1993; Erdem and Bingöl, 1997; Uygun and Solakoğlu, 2002), but as yet there have been no detailed mineralogical and geochemical studies focused on understanding the genesis of the hydrous Al-silicate minerals. The alteration processes that formed the metamorphic-hosted pyrophyllite-dickite association are known from a small number of studies (*e.g.* Espenshade and Potter, 1960; Sykes and Moody, 1978). This study is designed to

* E-mail address of corresponding author:
bozkaya@cumhuriyet.edu.tr
DOI: 10.1346/CCMN.2007.0550409

Copyright © 2007, The Clay Minerals Society

help understand the formation, origin, paragenetic relations and vertical distributions of pyrophyllite-dickite in terms of mineralogical and geochemical properties, provides new data and interpretations and constructs a genetic model for the HASD deposit.

REGIONAL GEOLOGICAL SETTING

It is widely accepted that the present geology of Turkey, constituting part of the Alpine Orogenic Belt, was exposed by the convergence between Laurasia and Gondwana due to the closure of the Tethyan Seaway in the Mesozoic and early Cenozoic (*e.g.* Şengör and Yılmaz, 1981). The geology of southeastern Anatolia (Figure 1a) consists of three roughly East–West-trending tectonic zones, the Southeast Anatolian Autochton (Arabian Platform), the imbrication zone and the nappe region covering the Pütürge metamorphic rocks (Figure 1b), which are separated from one another by major thrusts (Yılmaz, 1993).

The Pütürge HASD is found within Cambrian–Permian metamorphic rocks, called the Pütürge Metamorphic Massif (Yazgan, 1981; Yılmaz, 1993) or Pütürge Metamorphites (Bozkaya *et al.*, 2001), which consist, from bottom to top, of augen gneiss, mica-gneiss/schist intercalated with amphibolite, amphibole-gneiss/schist, granitic gneiss, kyanite-muscovite gneiss and calcschist/marble (Yazgan, 1981; Bozkaya *et al.*, 2001). The Pütürge Metamorphites initially underwent amphibolite-facies metamorphism and then greenschist-facies metamorphism that represent the northernmost extensions of the metamorphic basement of the Arabian platform to the south (Yazgan and Chessex, 1991; Bozkaya *et al*., 2001).

The Pütürge metamorphic suite is surrounded by the Upper Cretaceous Elazığ Magmatics and Kömürhan ophiolite and Eocene volcanic-volcanoclastic rocks of Maden Unit with tectonic contact with unconformable and sedimentary rocks of the Southeastern Anatolian Autochthonous Unit. Of these, the Kömürhan ophiolite represents a classic ophiolitic mantle and crustal succession that formed in a supra-subduction spreading zone (Beyarslan and Bingöl, 2000). The Elazığ magmatic suite is related to arc magmatism and cuts the upper parts of the ophiolite sequence. It is composed predominantly of granitoid (diorite, tonalite, granodiorite), volcanic (basaltic pillow lava, andesitic lava flows) and andesitic pyroclastic-volcanoclastic rocks (Turan *et al.*, 1995; Beyarslan and Bingöl, 2000). The Maden Group consists, from bottom to top, of conglomerate-sandstone-shale, limestone-tuffite-shale/metashale, and slate/phyllite-metasandstone with crystallized limestone lenses and spilitic basalts. It developed in a back-arc extensional basin (Yılmaz, 1993; Yiğitbaş and Yılmaz, 1996) and has metamorphosed under the sub-greenschist-facies conditions in an anticlockwise *P-T-t* pathway (Bozkaya *et al.*, 2006).

SAMPLING AND ANALYTICAL PROCEDURES

Four sectors representing open mines with 1–5 km diameters, named Vaktik Tepe, Ümik Tepe, Keşen Tepe and Karataş Tepe from northwest to southeast, were studied in detail, and 100 altered rock and/or mineral samples were collected from trenches and open galleries. Samples were investigated by optical microscopy and field emission scanning electron microscopy (FE-SEM), X-ray diffraction (XRD), fluid inclusion, major, trace, rare earth element (*REE*) and stable isotope (O-H) geochemistry and K/Ar dating methods. Sample preparation, clay fraction separation, XRD and fluid-inclusion studies were performed at the Geological Engineering Department of Cumhuriyet University. The SEM images were captured at the University of Georgia (USA). Geochemical analyses and K/Ar dating were done by Activation Laboratories (Canada). Information on analytical accuracy, precision, reproducibility, standards and detection limits are available from this company (www.actlabs.com).

Micromorphological and textural features of various phyllosilicates were examined using a LEO 982 model FE-SEM. For sample preparation a SPI-MODULE Sputter Coater was used for Au-Pd alloy coating of samples with running conditions of 2 mbar and 15 mA, which provided 156 Å coating thickness in 50 s.

The XRD studies (CuKα, Rigaku DMAX IIIC) were used to determine submicroscopic minerals of whole-rock and clay-size fractions and for the calculation of semi-quantitative percentages of their mineral phases by the use of multi-component mixtures as external standards (Brindley, 1980). The XRD settings are given as 35 kV, 15 mA, slits (divergence = 1º, scatter = 1º, receiving monochromator = 0.30 mm) and scan speeds of 2º2θ/min and 1º2θ/min for whole-rock and oriented clay fractions, respectively. Polytype determination of pyrophyllite, kaolin and white K-mica and *b* cell dimensions of white K-mica were performed on the nearly monomineralic clay fractions. Diagnostic polytype reflections were measured as stated in Bailey (1988) and J.C.P.D.S. (1990). Quartz (59.97º2θ, d = 1.541 Å) was selected as an internal standard for the *b* dimension of phyllosilicate minerals. Clay fractions extracted by the sedimentation method to reveal mineralogical assemblages were prepared under normal (air dried), glycolated (placed in a desiccator at 60ºC for 16 h) and heating (at 490ºC for 4 h) conditions.

Fluid-inclusion studies were conducted on quartz crystals in samples collected from syngenetic silica veins contemporary with hydrous Al-silicate alteration. Microthermometric measurements were performed using a NIKON Labophot-pol microscope mounted with a LINKAM THMS-600 and TMS-92 freezing-heating stage and a long-distance LW40× objective lens. Liquid nitrogen was used for freezing. The heating rate was controlled manually with the help of a TMS-92 system in the range of 0.1 to 5.0ºC/min. Repeated

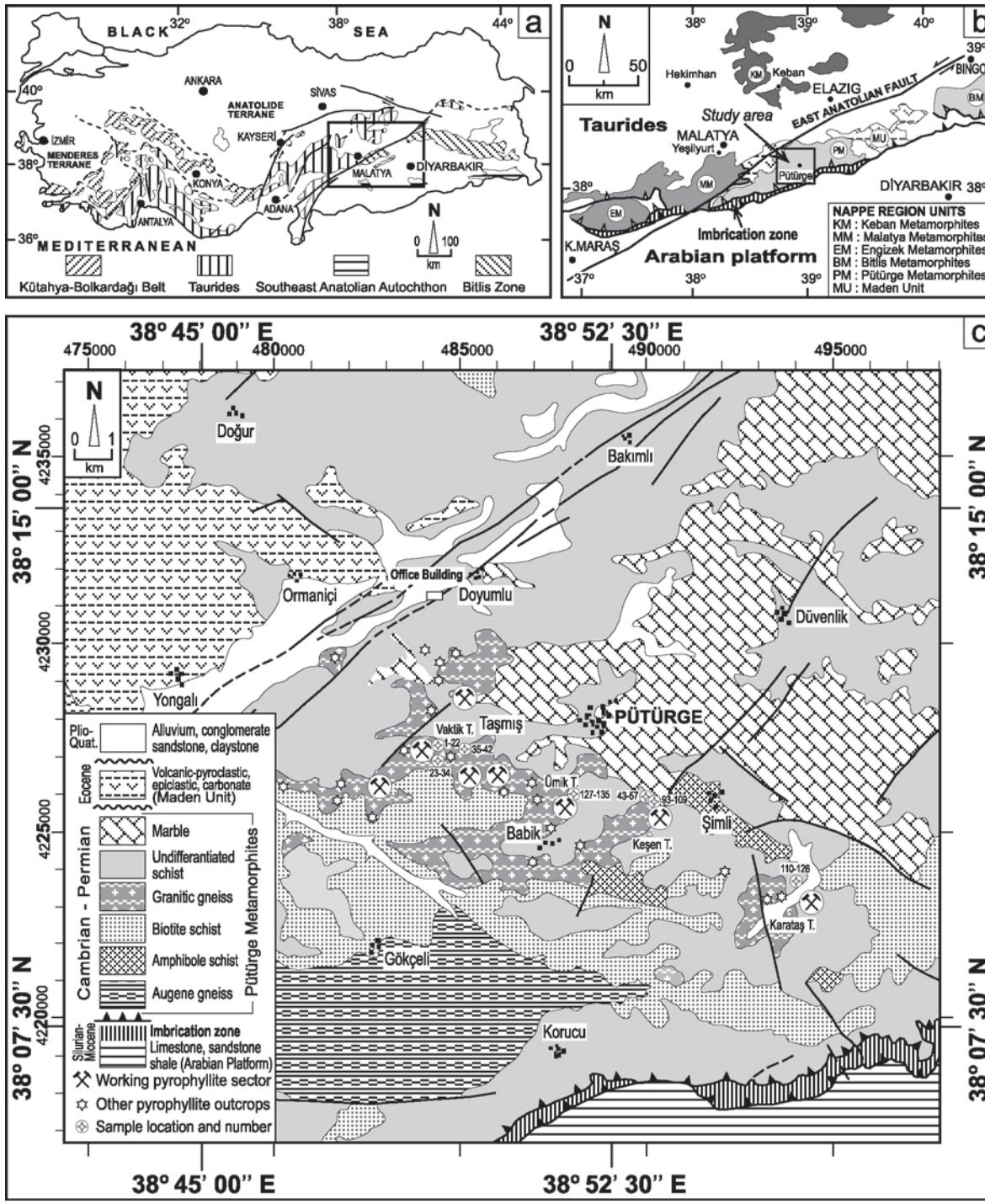

Figure 1. (a) Index tectonic map of southern Turkey, showing general geological divisions (simplified from Göncüoğlu, 1997); (b) regional geological sketch map of eastern-southeastern Anatolia, illustrating key tectonic units (compiled from Yılmaz, 1993); (c) geological map of the Pütürge area (modified from Yazgan, 1981), and sampling locations.

measurements showed that the error in the temperature determinations was <±0.5ºC for all three types.

Inductively coupled plasma (ICP) and inductively coupled plasma-mass spectrometry (ICP-MS) methods were used to analyze major and trace elements in the nearly pure pyrophyllite and dickite <2 μm fractions. The most aggressive technique employs a lithium metaborate/tetraborate fusion. The resulting molten bead is rapidly digested in a weak nitric acid solution to ensure that the entire sample is dissolved.

The ICP-MS instrument employs an argon plasma as the ionization source and a quadruple mass spectrometer to detect the ions produced. During analysis, the sample solution is nebulized into flowing argon gas and passed into an inductively coupled plasma. The gas and nearly everything in it is atomized and ionized, forming a plasma which is a source of both excited and ionized atoms. The positive ions in the plasma are then focused down a quadrupole mass spectrometer where they are separated according to mass, detected, multiplied and counted.

O-H isotope data were obtained from quartz, pyrophyllite and dickite minerals, using a Finnigan Mat 251 mass spectrometer and are stated as the δ permil notation with respect to the V-SMOW standard. Analytical precisions are of ±0.3‰ for oxygen and ±0.2‰ for hydrogen of pyrophyllite and dickite and of ±0.3‰ for oxygen and ±1‰ for hydrogen of fluid inclusions in quartz. Oxygen was analyzed by attacking the mineral powders by fluorination (BrF_5) at 650ºC in nickel pumps following the procedure of Clayton and Mayeda (1963). Hydrogen was analyzed by dehydration of pyrophyllite and dickite at 1400ºC for 20 min, purifying the water extracted by using cold traps. Hydrogen isotope analyses were performed on inclusion fluids released from the separated quartz grains by thermal decrepitation in which extracted water vapor was converted to hydrogen gas, and the δD of each sample was detected.

K/Ar dating was applied to alunite samples without other K minerals (micas, K-feldspar etc.). The K concentration was determined by flame atomic absorption spectrophotometry. The Ar analysis was performed using the isotope dilution procedure on noble gas mass spectrometry. The K/Ar dating method includes the high-precision determination of the concentration of the mother and daughter isotopes and apparent age calculation.

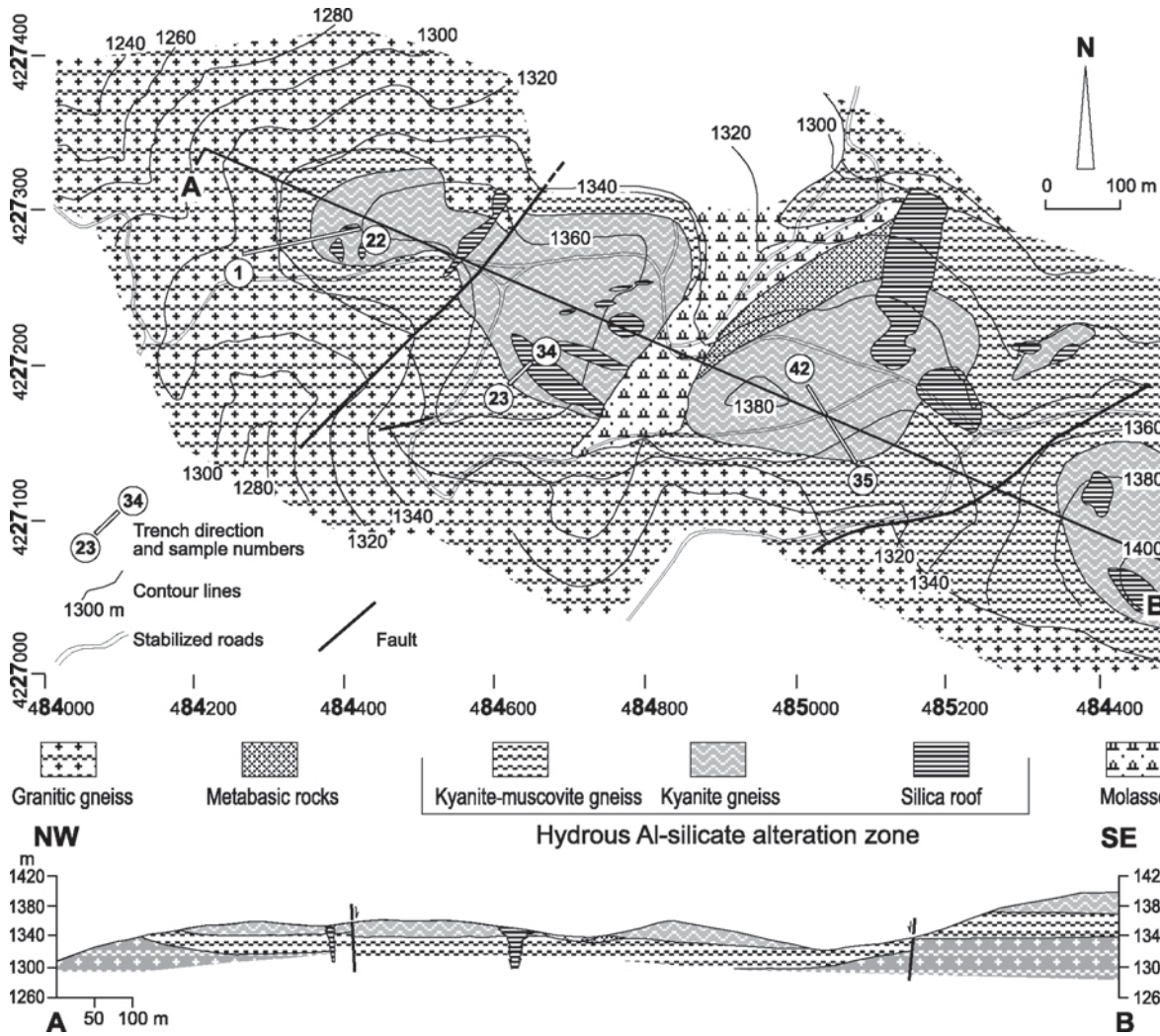

Figure 2. Geological sketch-map and section of the Vaktik Tepe sector in the Pütürge HASD (modified from Yılmaz *et al.*, 1993).

RESULTS AND DISCUSSION

Stratigraphy and lithology

The Pütürge HASD is located 3 km south of the Pütürge district and forms an alteration zone ~15 km long with a NW–SE trend (Figure 1c). Mica-gneiss/schist is a widespread lithology, but augen gneiss and metacarbonate rocks were observed in the southern and northern parts of the study area. Granitic gneiss crops out along the zones with a NW–SE orientation.

The Vaktik Tepe sector, one of the four open mines, is the largest deposit and is well known in ore geology. The alteration zones 20–50 m thick and 0.5–2 km^2 in area, are located at the highest topographic levels and are surrounded by kyanite-bearing gneissic metamorphic rocks (Figure 2). The deposits include silica veins and were covered by silica roofs ~3–10 m thick and 20–250 m long.

The neighboring rocks of the HASD are white-gray and partly mylonitized granitic gneiss with crenulation folds (Figure 3a) and greenish white muscovite gneiss with kyanite (Figure 3b). These rocks contain rare 1–10 m thick metabasic lenses (Figure 3c) and 10–30 cm thick silica veins and/or lenses (Figure 3d) including prismatic black tourmaline with 1–10 mm pinkish-gray specularite crystals. Muscovite gneiss generally contains disseminated and plastered hematite and goethite occurrences within levels ranging from 0.3 to 2 m thick, particularly in the upper parts. The bluish-white and greenish-white pyrophyllitic zones range from 25 to 50 m thick, and are overlain by a white-gray silica roof varying between 3 and 10 m thick at the uppermost levels.

Petrography

Based on optical microscopy studies, the granitic gneiss has a blasto-granular texture at the bottom and a mylonitic texture in the upper parts. Samples contain mainly quartz, kaolinized and sericitized orthoclase, albite, muscovite, sericite and tourmaline. Kyanite-bearing rocks overlying the granitic gneiss, the source rocks of pyrophyllite, are composed of kyanite-muscovite gneiss, kyanite gneiss and kyanite-quartzite. Silica lenses and veins associated with these rocks consist of quartz, tourmaline, specular hematite and muscovite.

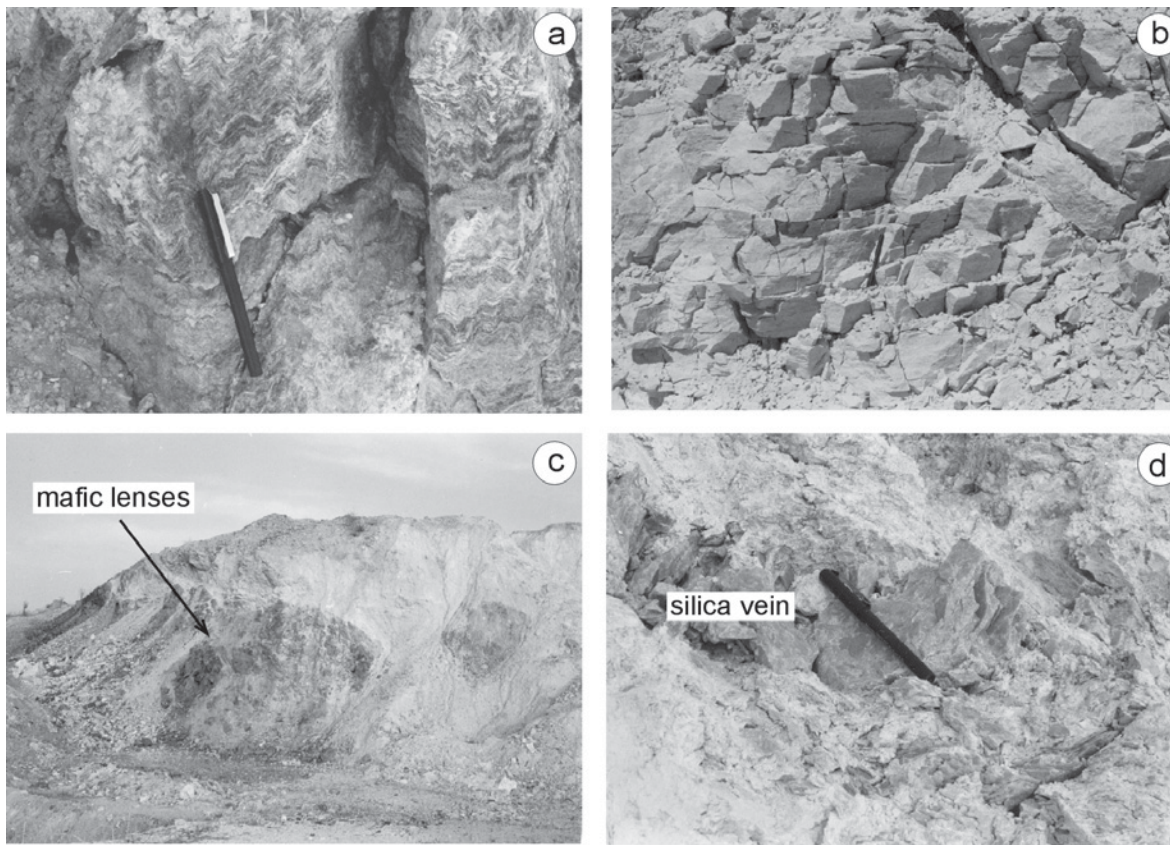

Figure 3. Typical field appearances in the Karataş Tepe sector of the Pütürge HASD: (a) gray-black to cream, mylonitic, granitic gneiss including typical banded crenulation folds; (b) greenish-white, abundantly cracked and foliated kyanite-muscovite gneiss transformed into hydrous Al-silicate minerals; (c) dark green to brown metabasic rock lenses or blocks within the green to white muscovite gneiss (Keşan Tepe sector); (d) gray syngenetic hydrothermal silica veins within the greenish white and altered gneiss with yellowish limonitic levels in some places.

Rarely observed metabasic rocks are characterized by albite-chlorite-schist and chlorite-muscovite-schist indicating the subgreenschist facies.

In thin-sections cut parallel to the *c* crystallographic axis, pyrophyllite has a fibrous form in all photomicrographs. Kyanite in the most of samples was transformed to pyrophyllite and their relics remained within the pyrophyllitic zones (Figure 4a). Dickite and pyrophyllite are seen as a fine-grained groundmass being formed in fractures or cleavage planes on kyanite (Figure 4b). Dickite is common both as a filling of fissures and pores in the rock, and as a replacement of kyanite relics (Figure 4c). Dickite also occurs as parallel intergrowths with pyrophyllite plates (Figure 4d). Topaz, fine-grained white K-mica, diaspore, alunite, gibbsite and dumortierite accompany the pyrophyllite and dickite. Topaz exhibits rounded to tabular prismatic aggregates (Figure 4e). Diaspore was detected as anhedral grains within and surrounding kyanite and anhedral-subhedral dumortierite was found in the pyrophyllitic zones (Figure 4f). Subhedral-euhedral prismatic alunite shows syngenetic occurrences with pyrophyllite, but they were cut and replaced by dickite (Figure 4g). Gibbsite was developed mainly within the fracture-filling dickite zones (Figure 4h). Acicular-prismatic tourmaline occurs in granitic gneiss and silica veins.

Investigations by SEM of two altered samples (PP-25, kyanite-muscovite gneiss; PP-52 quartz kyanite gneiss) show that pyrophyllite and dickite generally have few characteristic features (Figure 5a). Pyrophyllite occurs mainly as coarse-grained scaly aggregates (Figure 5b) with a platy cleavage (Figure 5c). Platy particles with angular borders are ~0.5 μm thick and 2–10 μm long (Figure 5d), which are slightly larger than those of volcanic-hosted specimens described from Japan (Sudo *et al.*, 1981).

In the other sample, platy dickite shows a finely laminated layer structure, with sizes in the range 0.1–0.2 μm thick and 1–5 μm long (Figure 5e). Dickite is also found as folded flakes with euhedral edges (Figure 5f), corresponding to a stage of rock deformation related to the exhumation of the metamorphic series. Dickite has a loose packing texture that is different from the tightly compacted texture of pyrophyllite, and these phases originate in diverse environments (*e.g.* Keller, 1976, 1978; Gençoğlu *et al.*, 1989; Yalçın, 1991; Yalçın and Bozkaya, 2003).

XRD

Fine-grained phases such as white K-mica, paragonite, pyrophyllite, dickite, alunite, diaspore, hematite and goethite were identified by powder XRD (Figure 6a–c). Tourmaline in silica veins has a dravitic composition. In order of abundance, the most common clay fraction assemblages can be listed for stages of pyrophyllitic and kaolinitic alterations as below (Figure 7): pyrophyllite + dickite + white K-mica + paragonite; pyrophyllite + dickite + white K-mica + paragonite + I-S + goethite; pyrophyllite + dickite; dickite + pyrophyllite + diaspore + gibbsite; dickite + pyrophyllite + alunite and/or crandallite/goyazite, white K-mica + paragonite + dickite + chlorite; white K-mica + dickite + chlorite; white K-mica + paragonite and white K-mica + pyrophyllite + dickite.

Pyrophyllite is a 2-layer monoclinic ($2M_1$) phase with a d_{060} value of 1.494 Å and poorly resolved doublets at 2.55–2.57 Å and 2.086–2.059 Å (Figure 8a). Kaolin occurs as a $2M_1$ polytype with typical *d* values of 2.94, 2.80, 2.32 and 2.21 Å and relative intensities that agree with the data for dickite (Figure 8b). Fine-grained white K-micas are $2M_1$+1*M* in granitic gneiss and $2M_1$ in muscovite gneiss with kyanite. Chlorite in the metabasic rocks occurs as the *IIb* polytype. The b_0 cell dimension of white K-micas varies between 8.990 and 9.019 Å (mean 9.004 Å), indicating a nearly ideal muscovitic composition.

The d_{001} values of muscovite (9.951–10.004 Å) and paragonite (9.618–9.675 Å) for eight muscovite + paragonite associations plot below the ranges suggested by Zen and Albee (1964) except for three samples. The paragonite component (or interlayer Na content) of the samples varies from 13 to 19% (mean 16%), suggesting temperatures of formation of <350ºC (Chatterjee and Flux, 1986).

Dickite is found in all samples and is the main mineral together with pyrophyllite in the region. According to the vertical distribution of hydrous Al-silicate occurrences in the Vaktik Tepe sector (Figure 9), kaolin occurrences begin from granitic gneiss and their amounts increase towards upper parts. Pyrophyllite first appears in kyanite-muscovite gneiss and increases in kyanite gneiss.

Fluid-inclusion studies

Fluid-inclusion studies were carried out on seven quartz samples taken from silica lenses and veins within

Figure 4 (*facing page*). Optical photomicrographs of altered samples from the Pütürge HASD (Mineral abbreviations: Prl = pyrophyllite, Dkt = dickite, Alu = alunite, Ky = kyanite, Dsp = diaspore, Du = dumortierite, Qtz = quartz, Ms = muscovite, Gbs = gibbsite, To = topaz. All photomicrographs were obtained under crossed nicols). (a) Relict kyanites transformed into diaspore within the pyrophyllitic zones of quartz kyanite gneiss; (b) kaolinized kyanite pseudomorphs and platy pyrophyllites developed on both cleavage planes and cracks of kyanites in the mica-schist; (c) platy pyrophyllite replacing kyanite, and crack-filling and platy-fan shaped dickites in the gneiss; (d) dickite fans parallel to pyrophyllite plates and also kyanite pseudomorphs in the quartzites; (e) pyrophyllite forming kyanite pseudomorphs with the rounded topaz aggregates in the gneiss; (f) irregularly shaped diaspore and dumortierite within kyanite in the muscovite gneiss; (g) prismatic alunites associated with kyanite, pyrophyllite and diaspore in the quartzite; (h) coarse-grained gibbsite plates within the fine-grained dickites, cutting pyrophyllite plates.

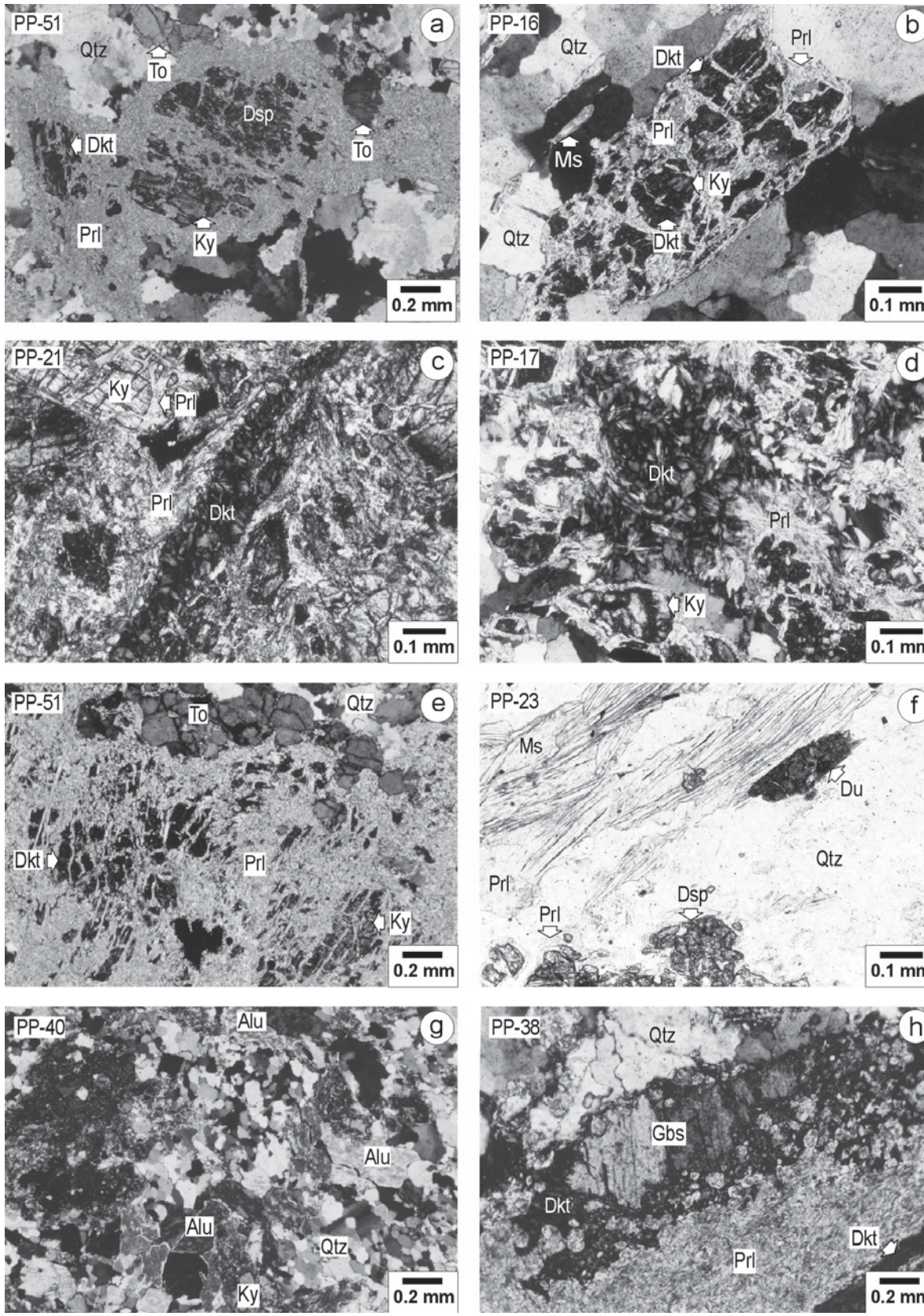
PP-51
a
Qtz
To
Dsp
Dkt
To
Prl
Ky
0.2 mm
PP-16
b
Qtz
Dkt
Prl
Prl
Ms
Ky
Qtz
Dkt
0.1 mm
PP-21
c
Ky
Prl
Prl
Dkt
0.1 mm
PP-17
d
Dkt
Prl
Ky
0.1 mm
PP-51
e
To
Qtz
Dkt
Prl
Ky
0.2 mm
PP-23
f
Ms
Du
Qtz
Prl
Dsp
Prl
0.1 mm
PP-40
g
Alu
Alu
Alu
Qtz
Ky
0.2 mm
PP-38
h
Qtz
Gbs
Dkt
Dkt
Prl
0.2 mm

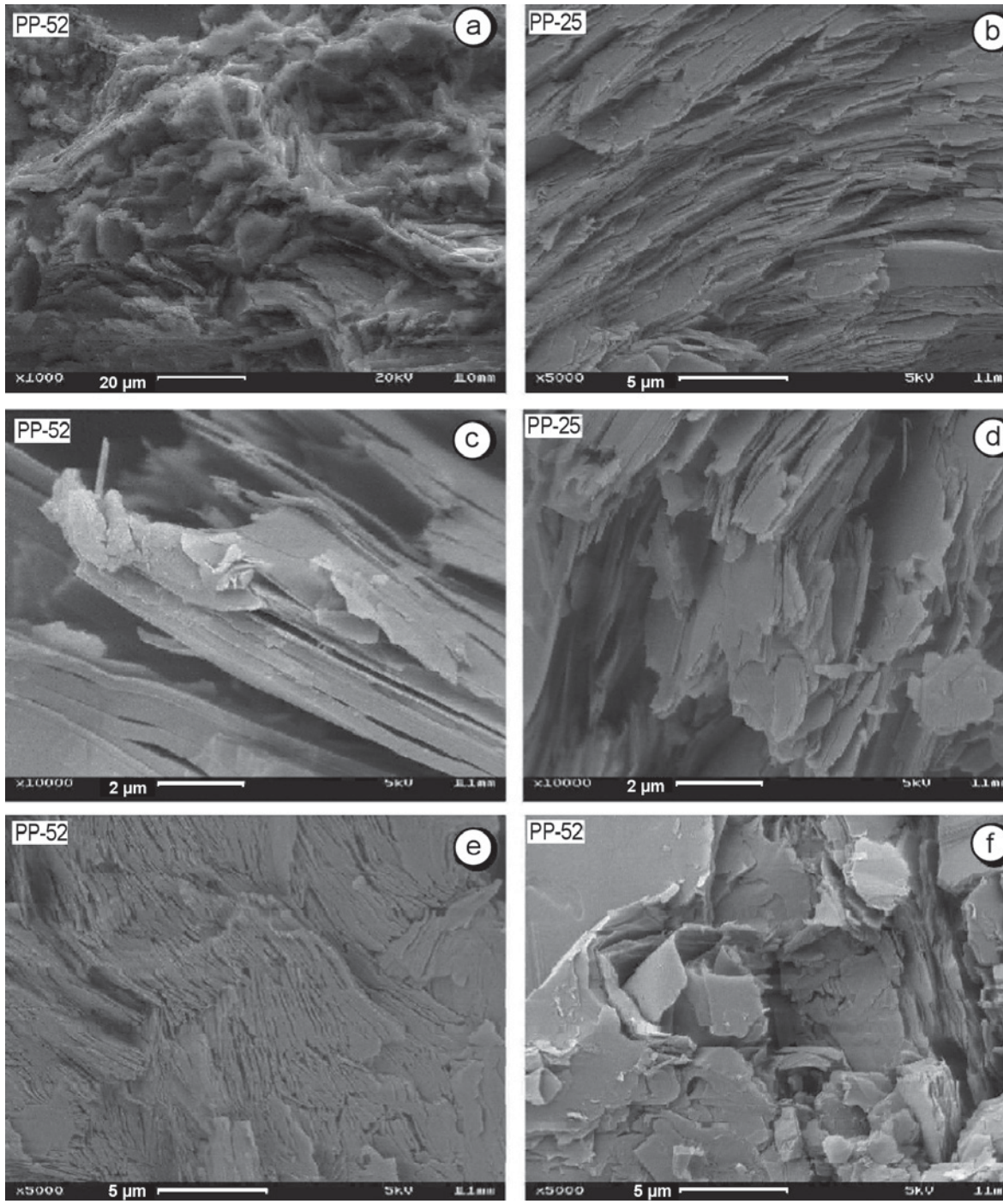

Figure 5. SEM images of altered kyanite gneiss from the Pütürge HASD: (a) general appearance of pyrophyllite and dickite aggregates; (b) pyrophyllites showing foliated lamellae; (c) enlarged view of pyrophyllites with perfect platy cleavage; (d) pyrophyllite plates with angular borders; (e) finely laminated layers of vermiform dickites with loose packing; (f) dickites as curved fine flakes with disorder edges.

several sectors of the Pütürge HASD (Table 1). The quartz crystals investigated include primary and secondary inclusions. Of these, the primary inclusions are more widespread and have mostly circular and ellipsoidal shapes. The secondary inclusions were formed along micro-fractures within the quartz crystals and are circular, pear-shaped, elongated ellipsoidal and tubular. This suggests that the primary inclusions represent the fluid responsible for quartz formation while the secondary inclusions represent the fluid of later episodes. Both

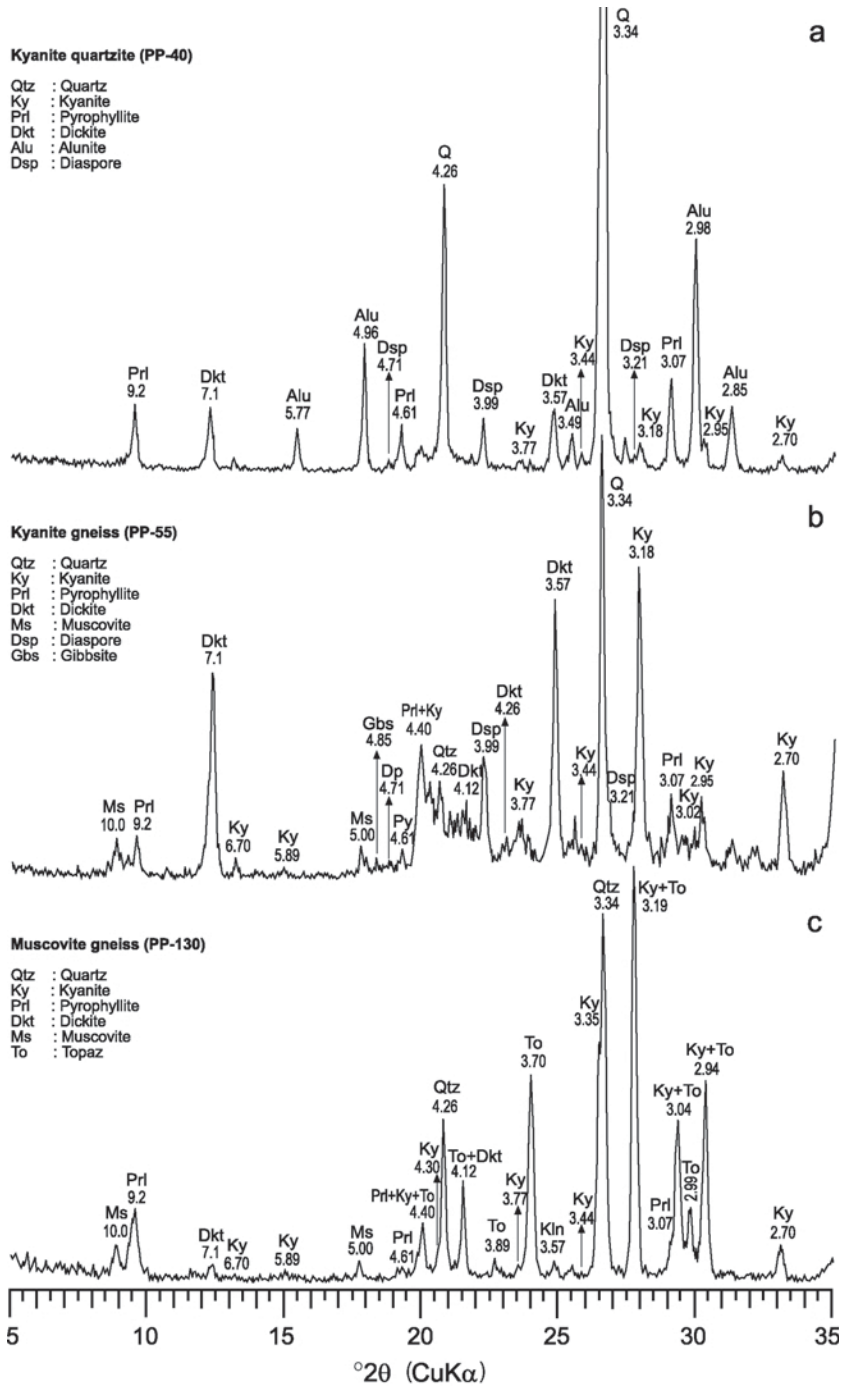

Figure 6. Representative bulk-rock XRD patterns of pyrophyllitized/kaolinized metamorphic rocks from the Pütürge HASD: (a) kyanite-quartzite; (b) kyanite gneiss; (c) muscovite schist/gneiss.

types of inclusions are three-phase inclusions containing aqueous + CO_2 + gas at room temperature. The volumes of liquid CO_2 + gas phases were estimated to be between 5 and 10%.

The first melting temperature values between −57.0 to −56.0ºC are in accordance with the melting temperature of CO_2 (Shepherd *et al.*, 1985). The measured clathrate melting temperature values range from 2.5 to 5.2ºC (mean 3.5ºC), indicating that the salinity of the fluids is in the range 9.0−12.0 NaCl % (mean 11 NaCl %) equivalent.

The CO_2 phases were homogenized at ~31ºC and the final homogenization temperatures ranged from 110.2 to 245.3ºC averaging 148.6ºC for primary inclusions, and from 74.1 to 110.1ºC, averaging 93.5ºC, for secondary

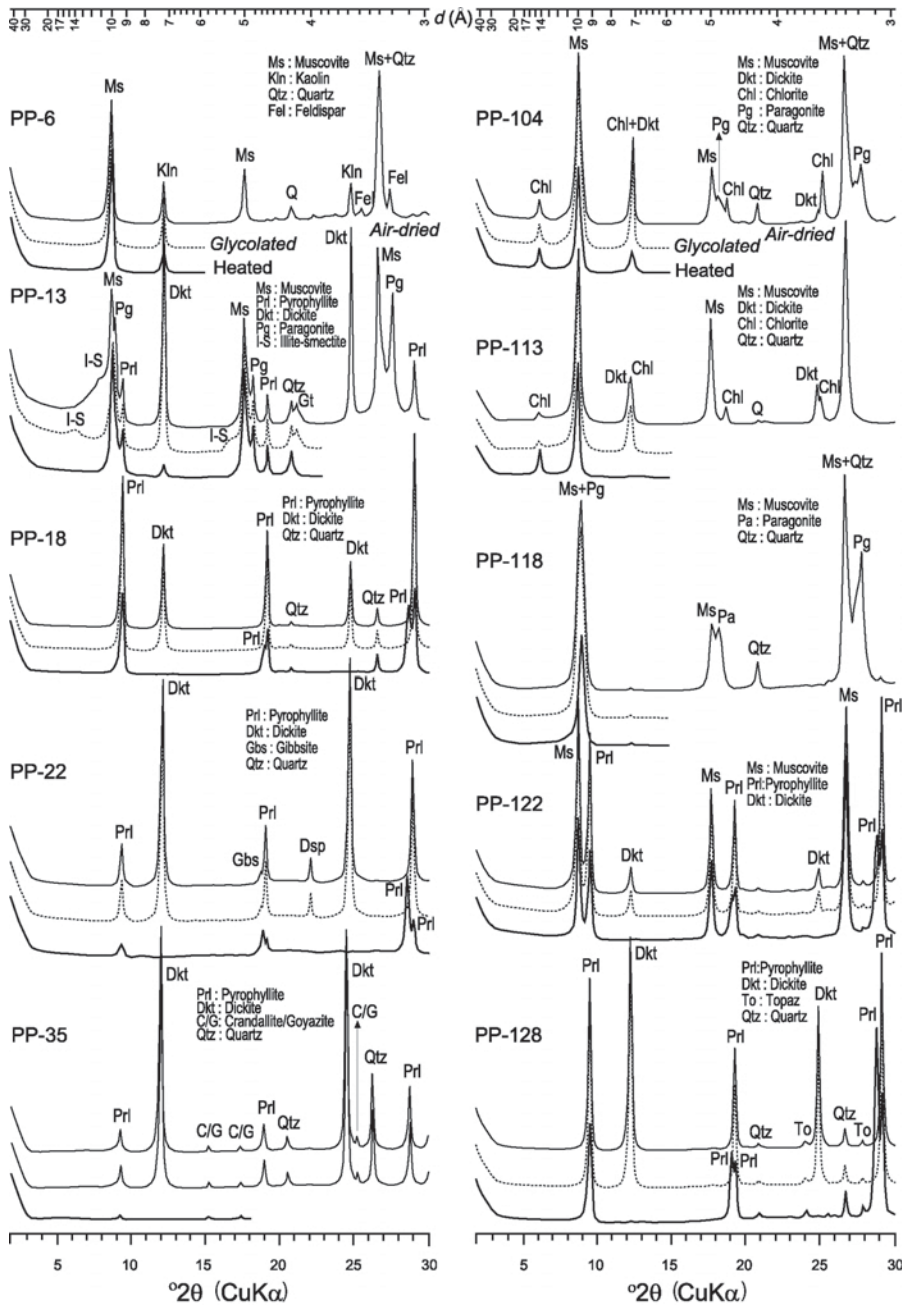

Figure 7. XRD patterns of some selected clay fractions from the Pütürge HASD.

inclusions (Figure 10). These results imply that the temperatures of fluids were high in the earlier stages and lower in the later episodes. The temperatures of early and later episodes could be evaluated as approximate temperatures of syngenetic formation of quartz with pyrophyllite and of secondary tectonic activity as indicated by fluid inclusions along fractures with dickite formation, respectively. However, relatively lower temperature values than those expected of the fluid inclusions for the pyrophyllite-bearing assemblages may be related to both precipitation of quartz after pyrophyllite occurrences and to various thermodynamic parameters – such as total pressure, water pressure, oxygen fugacity, activities of oxides, Fe differentiation *etc*. – that can cause variations in temperature (*e.g.* Evans and Guggenheim, 1988).

Mineral geochemistry

Geochemical analyses of separated pyrophyllitic and kaolinitic fractions are given in Tables 2 and 3. Contents

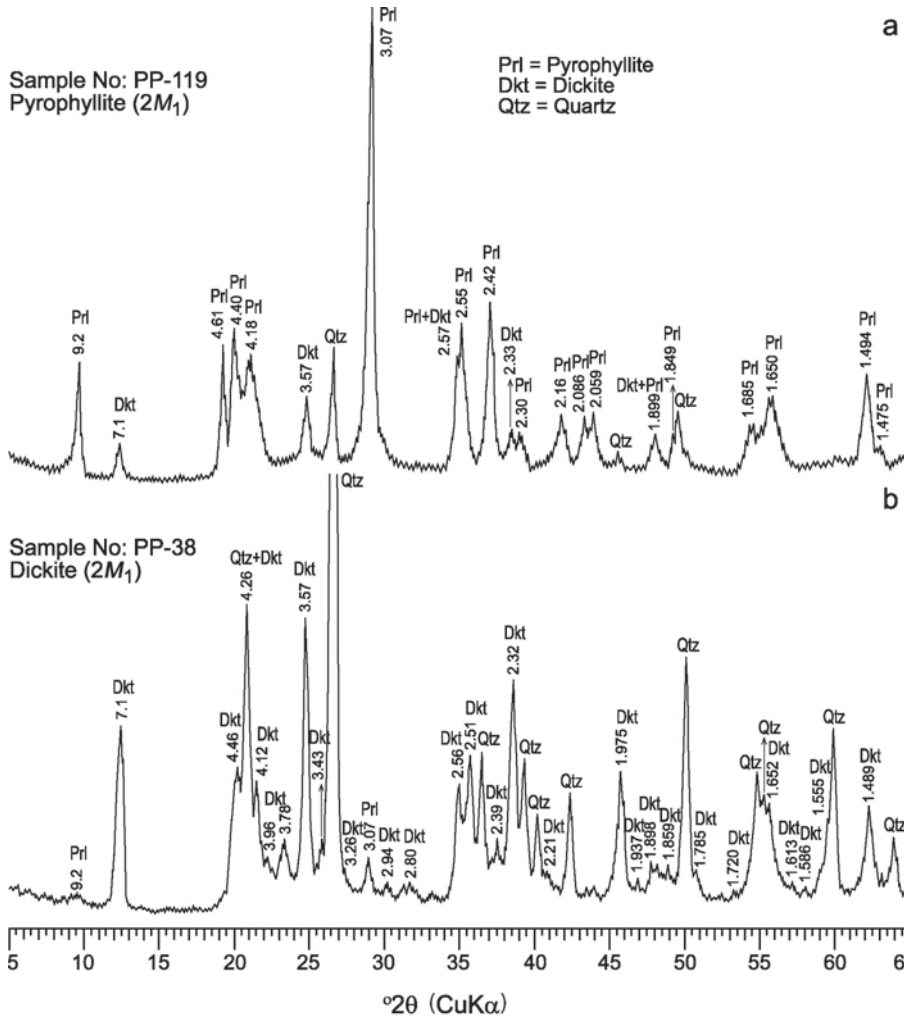

Figure 8. XRD patterns of random mounts representing polytypes from the Pütürge HASD: (a) pyrophyllite-rich fraction; (b) dickite-rich fraction.

of TiO_2, ΣFe_2O_3, MgO, CaO, Na_2O, K_2O and P_2O_5 are low in both nearly pure pyrophyllite (PP-106) and dickite (PP-22) minerals. Except for P_2O_5, these oxides are higher in pyrophyllite than in dickite. The SiO_2 concentration is low in dickite but it is high in pyrophyllite, and there is an inverse case for Al_2O_3 with regard to their ideal end-member compositions. These differences were caused by the existence of minor amounts of dickite and pyrophyllite in the pyrophyllite and dickite fractions, respectively. For this reason, the structural formulae of these minerals were not calculated. Ca, Na and K may indicate the presence of trace

Table 1. Homogenization temperatures (T_H) of primary and secondary inclusions in the quartz veins from different sectors in the Pütürge HASD (n = measured number).

Sample no.	Sector	Homogenization temperatures (°C) — Primary inclusions — Range	Mean	n	— Secondary inclusions — Range	Mean	n
PP-3	Vaktik Tepe	120.7–147.9	136.5	14	78.3–105.2	92.6	13
PP-10	Vaktik Tepe	144.4–220.2	172.6	12	74.1–100.4	83.9	7
PP-93	Keşen Tepe	110.2–141.7	126.0	2	78.3–100.2	87.2	16
PP-98	Keşen Tepe	121.9–122.3	122.1	2	89.9–109.2	99.9	13
PP-112	Karataş Tepe	119.2–245.3	165.1	14	85.2–110.1	102.8	10
PP-131	Ümik Tepe	115.9–128.1	121.3	7	86.5–104.7	93.7	11

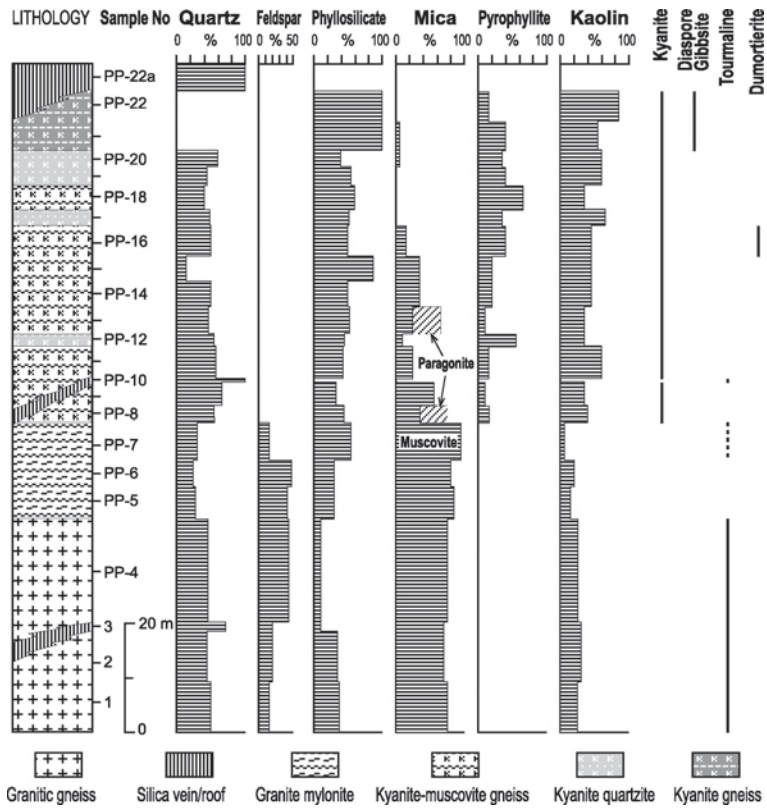

Figure 9. Vertical distributions of rocks and minerals in the measured section from Vaktik Tepe sector in the Pütürge HASD.

amounts of mica and/or feldspar phases rather than the incorporation of these elements into dickite and pyrophyllite structures.

Two further samples, pyrophyllite-rich (PP-49) and dickite-rich (PP-35) fractions, contain dickite and pyrophyllite, respectively, plus quartz as well as trace amounts of crandallite/goyazite as determined by XRD. The relatively high concentrations of Ca, P and Sr can probably be explained as due to the presence of crandallite group minerals. The Sc, Pb, Zn, Bi, In, Sn, Mo, Be, Ag and Tl values are below detection limits and the U content is the same as for nearly pure pyrophyllite and dickite (Table 3). The transition metal, W, from granitoid elements, low-field strength elements except for Sr and high-field strength elements except for Nb, Y and Th are enriched in pyrophyllite, whereas miscellaneous elements are decreased in the nearly pure pyrophyllite fraction. In addition, crandallite/goyazite-

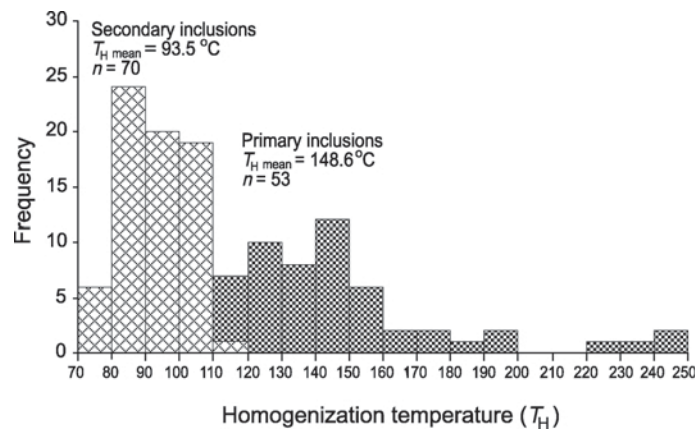

Figure 10. Frequency distribution histogram exhibiting values of homogenization temperature in the primary and secondary fluid inclusions from quartz minerals in the syngenetic silica veins of the Pütürge HASD.

Table 2. Major (wt.%) element compositions for the fractions rich in dickite and pyrophyllite from the Pütürge HASD (SFe_2O_3 as total Fe, LOI = loss on ignition).

	Pyrophyllite		Dickite	
Oxide %	PP-49	PP-106	PP-22	PP-35
SiO_2	66.26	62.08	51.54	54.58
TiO_2	0.077	0.019	0.003	0.094
Al_2O_3	20.60	29.22	37.08	30.87
ΣFe_2O_3	0.37	0.14	0.06	0.18
MnO	0.003	0.002	0.002	0.014
MgO	0.06	0.02	<0.01	0.10
CaO	0.15	0.07	0.06	0.56
Na_2O	0.09	0.18	0.07	0.11
K_2O	0.18	0.13	0.04	0.34
P_2O_5	0.13	0.03	0.14	0.90
LOI	6.38	7.05	10.76	11.67
Total	100.29	98.95	99.78	99.41

bearing pyrophyllite- and dickite-rich fractions have higher concentrations in some elements such as W, Sb, Sr, Ta and Th compared with nearly pure equivalents.

Chondrite-normalized (Sun and McDonough, 1989) trace element patterns of the pyrophyllitic and kaolinitic fractions are shown in Figure 11. Nearly pure pyrophyllite and dickite have a typically distinct depletion in P and Ti. They generally show enrichment in large ion lithophile (LIL) elements relative to high field strength (HFS) elements. The trace element content of nearly pure dickite is greater than that of nearly pure pyrophyllite. Both nearly pure minerals display clearly negative anomalies in K, P and Ti and positive anomalies in Ba, Sr and Tb. As for the crandallite/goyazite-bearing fractions, they show LIL element enrichment relative to their nearly pure equivalents.

According to chondrite-normalized *REE* element variations of the pyrophyllitic and kaolinitic fractions, the total amount of *REE* in the nearly pure phyrophyllite is smaller than nearly pure dickite and has a $1-2\times$ enrichment in *REE* (Figure 12). The overall *REE* trends of nearly pure minerals are quite different from each other with slightly negative Eu anomalies. The curve for nearly pure pyrophyllite is almost parallel to the normalization line, increasing slightly in light *REE* and decreasing in heavy *REE*. The crandallite/goyazite bearing fractions are richer in light *REE* than nearly pure equivalents. Nearly pure pyrophyllite clearly has smaller *REE* contents in comparison with those of volcanic-hosted pyrophyllites in the Roseki deposits (Terakado and Fujitani, 1998).

Relative to chondrite, the nearly pure dickite sample has a $4-42\times$ enrichment in *REE*. The values of North American Shale Composite (NASC) are situated between dickite and diagenetic kaolinite from eastern Taurus (Turkey). The *REE* concentrations of nearly pure dickite are greater for all elements except when compared with La, Yb and Lu in the Roseki kaolinite

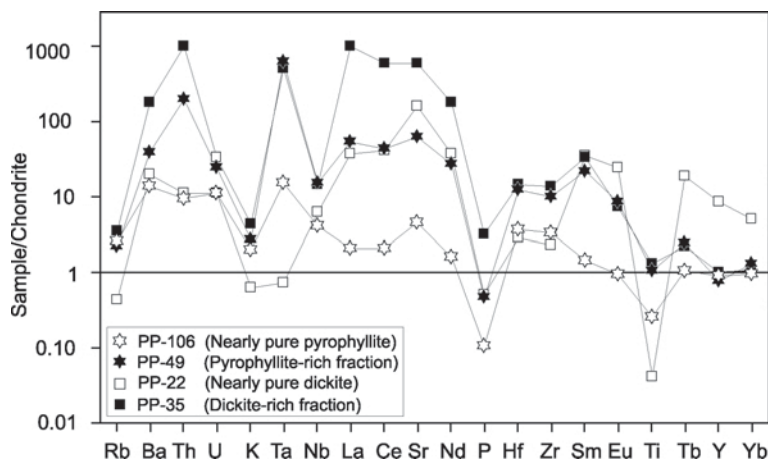

Figure 11. Chondrite-normalized multi-element variation diagram of pyrophyllitic and kaolinitic fractions from the Pütürge HASD (chondrite values from Sun and McDonough, 1989; Ho and Tm values from Haskin *et al*., 1968, and the other elements from Gromet *et al*., 1984 for NASC).

Table 3. Trace and *REE* (ppm) element compositions for the fractions rich in dickite and pyrophyllite from the Pütürge HASD.

Element	Pyrophyllite		Dickite	
(ppm)	PP-49	PP-106	PP-22	PP-35
Cr	93	60	55	101
Ni	<20	35	<20	<20
Co	26	64	3	32
Sc	4	<1	<1	2
V	21	12	6	46
Cu	<10	21	<10	<10
Pb	<5	<5	<5	21
Zn	<30	<30	<30	<30
Bi	<0.1	<0.1	<0.1	1.2
In	<0.1	<0.1	<0.1	<0.1
Sn	<1	<1	<1	1
W	1270	206	11.9	1250
Mo	<2	<2	<2	<2
As	72	7	17	29
Sb	11.8	1.0	0.2	9.2
Ge	1.6	1.2	1.7	4.1
Be	<1	<1	<1	<1
Ag	<0.5	<0.5	<0.5	<0.5
Rb	5	6	1	8
Cs	0.7	0.5	0.1	0.2
Ba	96	33	47	426
Sr	457	33	1170	4360
Tl	0.10	<0.05	<0.05	0.26
Ga	15	6	2	25
Ta	8.57	0.21	<0.01	6.99
Nb	3.7	1.0	1.5	3.5
Hf	1.3	0.4	0.3	1.5
Zr	39	13	9	53
Y	1.2	1.4	13.5	1.6
Th	5.76	0.28	0.33	29.2
U	0.19	0.09	0.09	0.26
La	12.5	0.49	8.88	237
Ce	26.6	1.25	25.8	368
Pr	3.00	0.17	3.68	32.5
Nd	12.5	0.75	17.6	84.9
Sm	3.42	0.22	5.37	5.07
Eu	0.496	0.056	1.410	0.425
Gd	1.59	0.25	6.20	1.42
Tb	0.09	0.04	0.71	0.08
Dy	0.27	0.23	3.02	0.33
Ho	0.05	0.05	0.49	0.07
Er	0.15	0.16	1.26	0.19
Tm	0.026	0.025	0.153	0.028
Yb	0.22	0.16	0.86	0.18
Lu	0.044	0.025	0.106	0.026

(Terakado and Fujitani, 1998), but less than that of diagenetic kaolinite from Eastern Taurus in Turkey (Bozkaya, 1995).

Stable isotope geochemistry

O-H isotope studies were carried out on three quartz crystals, two pyrophyllite samples and two dickite samples (Table 4). The $\delta^{18}O$ values for quartz range from +14.4 to +19.6‰ (SMOW), which are similar to those of metamorphic or sedimentary rocks (*e.g.* Hoefs, 1984). Thus, quartz veins and/or lenses should be considered as having a metamorphic source and are related to the surrounding Pütürge Metamorphites in the study area.

The $\delta^{18}O$ values for inclusion water in equilibrium with quartz were calculated using an equation of Zheng (1993a) and homogenization temperature values obtained in primary inclusions, which are dominant compared with secondary inclusions. The calculated $\delta^{18}O$ values vary from −2.4 to +2.55‰. The δD values for the inclusion water are clustered between −41.0 and −53.0‰ (SMOW). The lowest $\delta^{18}O$ and δD values of −2.4‰ and −53‰ were recorded from the sample of the Vaktik Tepe sector in the northwest part of the HASD zone, suggesting that the meteoric water was relatively dominant in a northwesterly direction. The $\delta^{18}O$ values are +17.2‰ and +17.8‰ for pyrophyllitic fractions, and +17.5‰ and +19.3‰ for kaolinitic fractions. While these values are quite similar, their δD values are different, ranging from −39.0 and −47.0‰, and −52.0 and −56.0‰, respectively.

The $\delta^{18}O$ and δD data for fluid inclusions in quartz, pyrophyllitic and kaolinitic fractions are presented in Figure 13 by adding lines and fields of various fluids as determined by some authors (Craig, 1961; Sheppard *et al.*, 1969; Sheppard, 1986; Urabe, 1987; Sheppard and Gilg, 1996). The isotopic values of fluid inclusions in quartz are found between the meteoric water line and the metamorphic water field, indicating that meteoric water was the major fluid component which originated from the interactions with metamorphic rocks during the hydrothermal stages. In addition, these isotopic values are also clustered between the meteoric water line and the magmatic water field, and partly within the field of Kuroko fluids, perhaps indicating that there were supplementary hydrothermal solutions with a magmatic source.

The $\delta^{18}O$ and δD data for the pyrophyllitic and kaolinitic fractions fall around the supergene−hypogene line, but the kaolinitic fractions are near to the weathering kaolinite line, which implies that the dickite was formed under shallow conditions with respect to the pyrophyllite.

The calculated isotopic ratios of fluids in equilibrium with pyrophyllite and dickite are obtained by using pyrophyllite-water and kaolinite-water fractionation factors as previously suggested (Zheng, 1993b; Gilg and Sheppard, 1996; Sheppard and Gilg, 1996). For the assumed temperatures of pyrophyllite (150ºC) and dickite (100ºC) formations, based on the results of fluid inclusion studies, comparable isotopic compositions of the coexisting water during precipitation of these minerals are obtained. The resulting isotopic ratios of the water plot close to the field of fluids in equilibrium with quartz veins in the $\delta D\delta^{18}O$ diagram (Figure 13). The results support precipitation of pyrophyllite at higher temperatures than dickite from

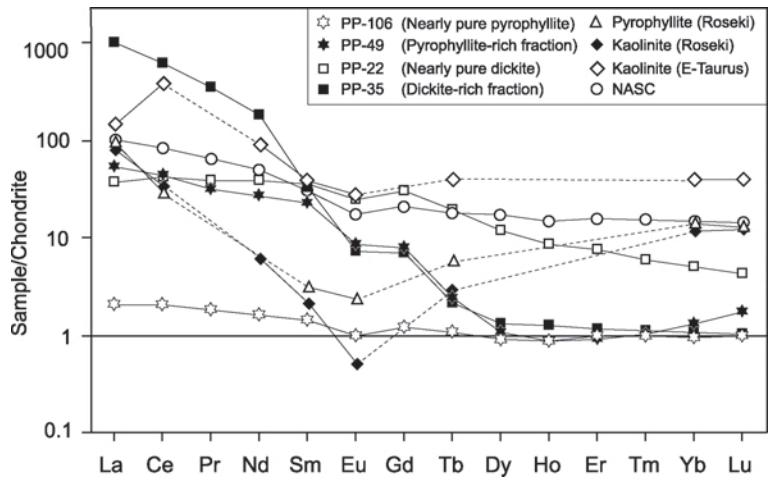

Figure 12. Chondrite-normalized *REE* spider diagram of pyrophyllitic and kaolinitic fractions from the Pütürge HASD (chondrite values from Sun and McDonough, 1989).

hydrothermal fluids derived from meteoric water equilibrated with the metamorphic host rocks at elevated temperatures. Furthermore, the isotopic composition of the alteration fluids may have changed with time and depth (*e.g.* Bechtel *et al.*, 1999), especially for dickite occurrences, during or after the uplift of the metamorphic unit.

K/Ar dating

The K/Ar ages of two alunite-bearing samples from the Vaktik Tepe sector are determined as 69−71 Ma (Table 5). Because pyrophyllite and alunite have syngenetic textural relationships, this suggests that both phases crystallized in early Maastrichtian (late Cretaceous) time. On the basis of the petrography, dickites must have occurred later.

Previous studies of K/Ar ages of the Pütürge Metamorphics (Yazgan *et al.*, 1983; Yazgan and Chessex, 1991) dated them as 85−76 Ma for amphibolites, 74−72 Ma for muscovite-schists, and 67−56 Ma for augen gneiss and biotite-mica-schists. The above authors concluded that the amphibolite age recorded amphibolite-facies metamorphism, depending on the extent of the earlier orogenesis, whereas schist and gneiss ages reflected the mica cooling that accompanied a pronounced pressure drop to greenschist facies possibly related to uplift and erosion during the arc-continent collision event. Thus, the hydrothermal alteration responsible for pyrophyllite developed may have occurred before uplift (high-temperature conditions), but dickite probably formed during or after uplift (low-temperature conditions).

Occurrence and origin

Pyrophyllite occurrences in the Pütürge developed as a result of temperature increases either along the shear zones between granitic and mica-gneisses (Yazgan and Chessex, 1991), or due to hydrothermal alteration (Erdem and Bingöl, 1997). Uygun and Solakoğlu (2002) pointed out that pyrophyllite can also occur in non-tectonic zones where it is generated from kyanite-bearing metamorphic rocks by retrograde metamorphism. Even though the hydrothermal alteration appears to be related to magmatic activities during late Cretaceous time (Yazgan and Chessex, 1991; Turan *et al.*, 1995; Önal and Bingöl, 1997), there is no direct evidence for magmatic fluids with respect to the isotopic data. Additionally, stable isotope and K/Ar dating indicate that the occurrence of pyrophyllite and dickite are probably related to the interactions of heated meteoric

Table 4. Isotope ratios of quartz, dickite and pyrophyllite minerals from the Pütürge HASD.

Sample no.	Sector	Material	$\delta^{18}O_{(SMOW)}$ (‰)	$\delta D_{(SMOW)}$ (‰)	Mean T_H (°C)	1000 lnα	$\delta^{18}O$ of fluids (‰)
PP-3	Vaktik Tepe	Quartz	14.4	−53	136.5	16.8	−2.4
PP-93	Keşen Tepe	Quartz	19.6	−41	126.0	17.9	1.7
PP−112	Karataş Tepe	Quartz	16.7	−44	165.1	14.2	2.5
PP-22	Vaktik Tepe	Nearly pure dickite	17.5	−56	–	–	–
PP-35	Vaktik Tepe	Dickite-rich fraction	19.3	−52	–	–	–
PP-106	Keşen Tepe	Nearly pure pyrophyllite	17.2	−39	–	–	–
PP-49	Keşen Tepe	Pyrophyllite-rich fraction	17.8	−47	–	–	–

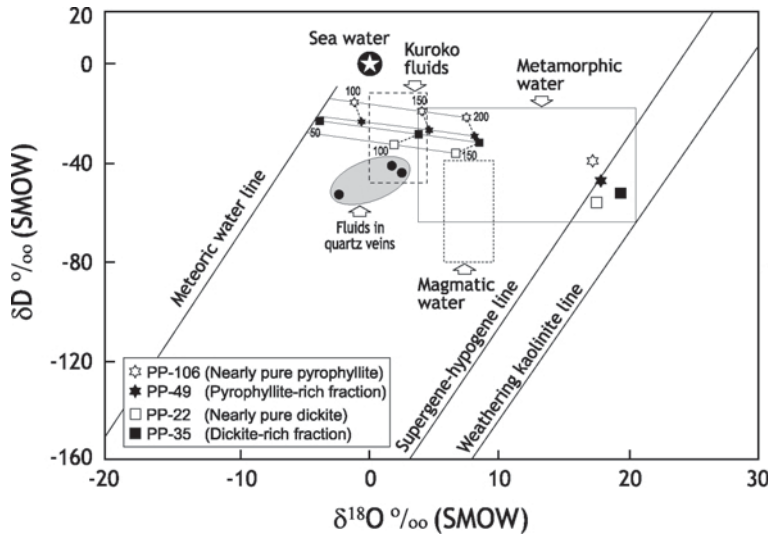

Figure 13. Plot of $\delta^{18}O$ *vs.* δD values for calculated isotope ratios of the fluids in equilibrium with pyrophyllite, dickite and quartz from the Pütürge HASD (Meteoric water line: Craig, 1961; supergene-hypogene and weathering kaolinite lines: Sheppard *et al.*, 1969; Sheppard and Gilg, 1996; the fields of sea water, metamorphic and magmatic waters: Craig, 1961 and Sheppard, 1986; Kuroko fluids: Urabe, 1987).

water and metamorphic rocks during late Cretaceous and later time.

Pyrophyllite is a stable mineral in the temperature range 275−350ºC in the Al_2O_3-SiO_2-H_2O system (Evans and Guggenheim, 1988). However, the formation temperature of pyrophyllite displaces to lower temperatures and it occupies a slightly broader temperature stability field when H_2O becomes progressively diluted by other fluid species, *e.g.* CH_4 and CO_2 (Evans and Guggenheim, 1988). On the other hand, silica-supersaturated fluids could result in the precipitation of pyrophyllite instead of kaolin at low-temperature conditions up to 100ºC during the hydrothermal alteration of silicates (Hemley *et al.*, 1980; Berman, 1988). Thus, in the study area, the presence of hydrothermal quartz veins including CO_2-rich fluids, and the existing SO_2 for the formation of alunite suggest that pyrophyllite occurred under relatively low-temperature conditions. Likewise, the homogenization temperatures of fluid inclusions in the quartz were determined as being <245ºC and the polytype of pyrophyllites is monoclinic, which is the low-temperature form (Eberl, 1979).

Based on the textural and paragenetic relationships from the Pütürge HASD, pyrophyllite, quartz, alunite, topaz, dravite, dumortierite, paragonite, chlorite and epidote minerals represent the relatively higher temperatures of formation, whereas dickite, quartz, diaspore, gibbsite, hematite and goethite reflect the lower-temperature parts of the hydrothermal stage of hypogene conditions. Schematic models of these alteration stages are presented in Figure 14. The alteration processes and reaction paths in the Pütürge HASD demonstrate that the integration of acidic fluids into host rock is directly related to the degree of fracturing and time. The pyrophyllitization followed by kaolinization appear to be a response to northwards subduction of the Arabian plate during the late Cretaceous and possibly back-arc extension during the Middle Eocene (Yiğitbaş and Yılmaz, 1996). Eocene-age kaolinitic alterations are common in the volcanic rocks surrounding both syenitic intrusions as well as metamorphic rocks in central eastern Anatolia (*e.g.* Yalçın and Bozkaya, 2003).

Hypogene mineral neoformation resulting from the effects of silica-saturated hydrothermal solutions can be explained by a series of reactions. Of these, pyrophyllite or pyrophyllite + topaz assemblages formed from kyanite in the muscovite gneiss:

$$\underset{\text{Kyanite}}{Al_2SiO_5} + 3H_4SiO_4 \rightarrow \underset{\text{Pyrophyllite}}{Al_2Si_4O_{10}(OH)_2} + 5H_2O$$

$$\underset{\text{Kyanite}}{2Al_2SiO_5} + 3H_4SiO_4 \rightarrow \underset{\text{Pyrophyllite}}{Al_2Si_4O_{10}(OH)_2} + \underset{\text{Topaz}}{Al_2SiO_4(OH)_2} + 4H_2O$$

Table 5. K/Ar isotope dating results of alunite-bearing rocks of the Pütürge HASD.

Sample no.	Mineralogical composition	$^{40}Ar_{rad}$ (nL/g)	K (%)	$^{40}Ar_{air}$ (%)	Age (Ma)
PP-32	Quartz+alunite+kyanite+pyrophyllite+dickite	4.80	1.73	22.5	71.3±2.0
PP-40	Quartz+alunite+kyanite+pyrophyllite+dickite+topaz	2.67	0.99	60.0	69.1±1.8

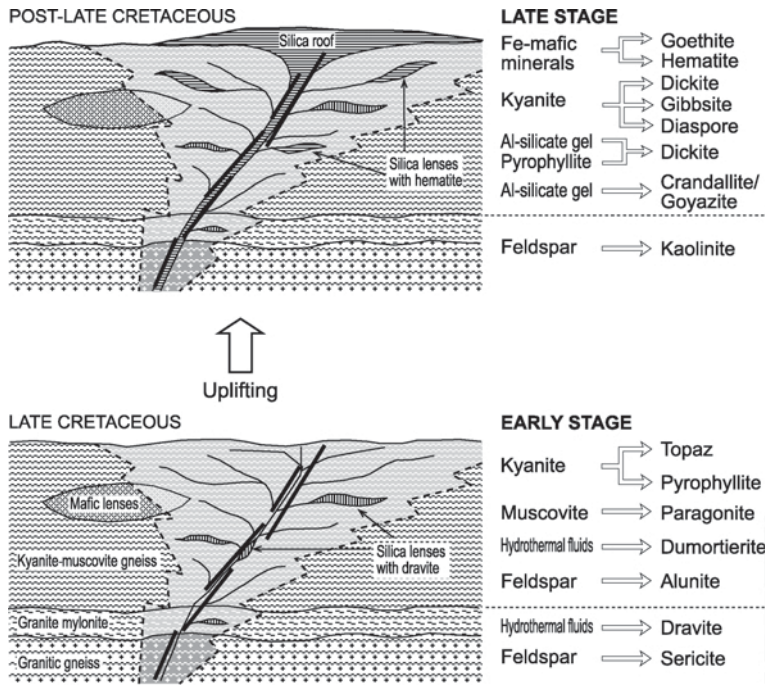

Figure 14. Cross-section of a metamorphic-hosted hydrothermal system and the evolution of silicate and oxide minerals throughout pyrophyllization and kaolinization in the Pütürge HASD.

The absence of feldspars in the altered muscovite gneiss suggests that alunites were derived from feldspars:

$$3(K,Na)AlSi_3O_8 + 2SO_2 + 4H_2O \rightarrow (K,Na)Al_3(SO_4)_2(OH)_6 + 9SiO_2 + 2H^+ + 2(K^+,Na^+)$$

Feldspar — Alunite — Quartz

Paragonite probably crystallized from muscovites during the hydrothermal alteration. The exchange of K is adequate for this reaction in which Na is provided by the alteration of feldspar:

$$KAl_3Si_3O_{10}(OH)_2 + Na^+ \rightarrow NaAl_3Si_3O_{10}(OH)_2 + K^+$$

Muscovite — Paragonite

Dravitic tourmaline and dumortierite may be precipitated in post-metamorphic silica veins by means of locally trapped boron-bearing fluids passing through granitic gneiss (*e.g.* Kawakami and Ikeda, 2003).

The following reactions seem to be valid for low-temperature hypogene conditions. For instance, dickite replacing kyanite that was a relic of pyrophyllite alteration is abundant and commonly associated with quartz and diaspore or gibbsite:

$$Al_2SiO_5 + H_4SiO_4 \rightarrow Al_2Si_2O_5(OH)_4$$

Kyanite — Dickite

$$2Al_2SiO_5 + 2H_4SiO_4 \rightarrow Al_2Si_2O_5(OH)_4 + 2(AlO.OH) + 2SiO_2 + H_2O$$

Kyanite — Dickite — Diaspore — Quartz

$$2Al_2SiO_5 + 2H_4SiO_4 + H_2O \rightarrow Al_2Si_2O_5(OH)_4 + Al_2(OH)_6 + 2SiO_2$$

Kyanite — Dickite — Gibbsite — Quartz

Dickite formed through the extension of pyrophyllite fibers that might confirm the following reaction was rarely observed in textural relations:

$$Al_2Si_4O_{10}(OH)_2 + H_2O \rightarrow Al_2Si_2O_5(OH)_4 + 2SiO_2$$

Pyrophyllite — Dickite — Quartz

Dickite together with gibbsite is found in the veins cutting the pyrophyllitic zones in some samples and the equation below is possible:

$$2Al_2Si_4O_{10}(OH)_2 + 3H_2O \rightarrow Al_2Si_2O_5(OH)_4 + Al_2(OH)_6 + 6SiO_2$$

Pyrophyllite — Dickite — Gibbsite — Quartz

Dickite cutting the pyrophyllitic zones seems to be developed from hydrous Al-silicate gel as formulated below:

$$Al_2(OH)_6.2Si(OH)_4 \rightarrow Al_2Si_2O_5(OH)_4 + 5H_2O$$

Al-silicate gel — Dickite

The remaining cations such as Ca, Sr and P that were not incorporated into the structures of other neoformed minerals were used to form crandallite/goyazite:

$$4Al_2(OH)_6.8Si(OH)_4 + Ca^{2+} + Sr^{2+} + 4P^{5+} \rightarrow Al_2Si_2O_5(OH)_4 + 6SiO_2 + (Sr, Ca)_2Al_6(PO_4)_4.2H_2O + 17H_2O + 14H^+$$

Al-silicate gel — Dickite — Quartz — Crandallite/goyazite

Kaolinite was developed from feldspar in the granitic gneiss:

$$2(K,Na)AlSi_3O_8 + H_2O + 2H^+ \rightarrow Al_2Si_2O_5(OH)_4 + 4SiO_2 + 2(K^+,Na^+)$$

Feldspar — Kaolinite — Quartz

Iron oxides are particularly characteristic minerals within the silica roof and were precipitated by hydrothermal fluids rich in Fe^{3+} released mainly from biotite-bearing schists in the lower parts of the metamorphic sequence:

$$2KFe_3(AlSi_3O_{10})(OH)_2 + 2H^+ \rightarrow 3Fe_2O_3 + 6SiO_2 + 3H_2O + 2Al^{3+} + 2K^+$$

Biotite — Hematite — Quartz

$$2KFe_3(AlSi_3O_{10})(OH)_2 + 2H^+ \rightarrow 6FeOOH + 6SiO_2 + 2Al^{3+} + 2K^+$$

Biotite — Goethite — Quartz

CONCLUSIONS

The results of this study are consistent with a two-stage sequence of hydrothermal processes developed within the metamorphic host rocks. The influences of the primary (late Cretaceous) and secondary (possibly Eocene) tectonic activities as indicated by fluid inclusions along fractures should be traced through the evolution of the Pütürge HASD.

Kyanite is the primary source material and it was converted to pyrophyllite and dickite by reaction with silicic, acid-rich fluids. Thin fibrous pyrophyllite plates developed along cleavage planes, fissures and edges of kyanite, whereas book-like dickite crystallized as both pore-fillings of rocks and as a replacement of kyanite.

Trace elements and *REE*s show characteristic patterns in the Pütürge HASD. Pyrophyllite has the most trace element-enriched features, whereas *REE*s were strongly concentrated in the structure of dickite. In addition, kaolin and pyrophyllite representing various environments such as hypogene and diagenetic processes as well as volcanic- or metamorphic-hosted occurrences can be distinguished by trace and *REE* patterns. On the basis of chondrite-normalized trace element patterns, nearly pure pyrophyllite and dickite display clear negative anomalies in K, P and Ti and positive anomalies in Ba, Sr and Tb. The *REE* trends of nearly pure minerals are quite different from each other with slightly negative Eu anomalies.

The homogenization temperatures of the fluids in syngenetic quartz veins indicate two-stage processes close to 150ºC and 100ºC, corresponding to pyrophyllitic and kaolinitic mineralization, respectively. The stable isotope compositions of the pyrophyllite- and dickite-rich fractions suggest that hydrothermal fluids originated as meteoric water and interacted with the metamorphic host rocks. The difference between the isotope ratios of both minerals can be explained by the formation of pyrophyllite at a higher (~50ºC higher) temperature than the dickite.

The characteristics obtained from this study provide additional petrogenetic characterization of anhydrous and hydrous Al-silicate and oxide minerals, which should enhance their use for mineral exploration purposes in the Bitlis-Pütürge metamorphic belt.

ACKNOWLEDGMENTS

This work was supported by project No. M-200 from the Research Fund of Sivas Cumhuriyet University, Turkey. We are indebted to Ahmet Gökçe for the instrumental facilities used in the fluid-inclusion study, Fatma Yalçın who kindly performed the XRD analysis, Hüseyin Yılmaz for his courtesy in sampling at the Pütürge mines, Ibrahim Altuntaş from the COŞTAŞ Mining Company for logistical help and Ö. Işık Ece for providing the SEM images. The authors are very grateful to Warren D. Huff who read and improved the text. We also acknowledge the critical remarks and helpful comments of reviewers Richard J. Merriman and Achim Bechtel, Associate Editor W. Crawford Elliott and Editor-in-Chief, Derek C. Bain.

REFERENCES

Aras, A. and Açıkgöz, F. (1992) *Mining geology of pyrophyllite field AR-43321 in the Malatya-Pütürge-Taşmış district and a report of pyrophyllite prospecting around Pütürge-Doğanyol.* General Directorate of Mineral Research and Exploration, Directorate of Malatya Region, Project no. 413, 20 pp. (in Turkish).

Bailey, S.W. (1988) X-ray diffraction identification of the polytypes of mica, serpentine, and chlorite. *Clays and Clay Minerals*, **36**, 193–213.

Bechtel, A., Savin, S.M. and Hoernes, S. (1999) Oxygen and hydrogen isotopic of clay minerals of the Bahloul Formation in the region of the Bou Grine zinc-lead ore deposit (Tunisia): evidence for fluid-rock interaction in the vicinity of salt dome cap rock. *Chemical Geology*, **156**, 191–207.

Berman, R.G. (1988) Internally-consistent thermodynamic data for minerals in the system Na_2O-K_2O-CaO-MgO-FeO-Fe_2O_3-Al_2O_3-SiO_2-TiO_2-H_2O-CO_2. *Journal of Petrology*, **29**, 445–522.

Beyarslan, M. and Bingöl, F. (2000) Petrology of a supra-subduction zone ophiolite (Elazığ, Turkey). *Canadian Journal of Earth Sciences*, **37**, 1411–1424.

Bozkaya, Ö. (1995) Mineralogy and geochemistry of sedimentary and very low grade metasedimentary rocks from Sarız-Tufanbeyli-Saimbeyli district, Eastern Taurus. PhD thesis, Cumhuriyet University, Sivas, Turkey, 334 pp. (in Turkish, with English abstract).

Bozkaya, Ö. and Yalçın, H. (2004a) New mineralogic data and implications for the tectono-metamorphic evolution of the Alanya Nappes, Central Tauride Belt, Turkey. *International Geology Review*, **46**, 347–365.

Bozkaya, Ö. and Yalçın, H. (2004b) Diagenetic to low-grade metamorphic evolution of clay mineral assemblages in Palaeozoic to early Mesozoic rocks of the Eastern Taurides, Turkey. *Clay Minerals*, **39**, 481–500.

Bozkaya, Ö., Yalçın, H. and Başıbüyük, Z. (2001) *Mineralogic-petrographic investigation of Malatya-Keban ve Pütürge metamorphites*. Research Fund of Cumhuriyet University, Sivas, Project No: M-163, 92 pp.

Bozkaya, Ö., Yalçın, H. and Dündar, M.K. (2006) *Clay mineral evolution in the rocks of Maden Group from Malatya-Pütürge area, Eastern Anatolia*. 4th Mediterranean Clay Meeting (MCM06), 5–10 September 2006, Middle East Technical University, Ankara, Turkey,

Abstracts, pp. 22–23.

Brindley, G.W. (1980) Quantitative X-ray mineral analysis of clays: Pp. 411–438 in: *Crystal Structures of Clay Minerals and their X-ray Identification* (G.W. Brindley and G. Brown, editors). Monograph **5**, Mineralogical Society, London.

Chatterjee, N.D. and Flux, S. (1986) Thermodynamic mixing properties of muscovite-paragonite crystalline solutions at high temperatures and pressures, and their geological applications. *Journal of Petrology*, **27**, 677–693.

Clayton, R.N. and Mayeda, T.K. (1963) The use of bromine pentafluoride in the extraction of oxygen from oxides and silicates for isotopic analysis. *Geochimica et Cosmochimica Acta*, **27**, 43–52.

Craig, H. (1961) Isotopic variations in meteoric waters. *Science*, **133**, 1702–1703.

Danış, M. (1978) *Pyrophyllite occurrences around Malatya city-Pütürge town-Babik village*. General Directorate of Mineral Research and Exploration, Directorate of Malatya Region, Project no. 18, 25 pp. (in Turkish).

Eberl, D. (1979) Synthesis of pyrophyllite polytypes and mixed layers. *American Mineralogist*, **64**, 1091–1096.

Erdem, E. and Bingöl, A.F. (1997) *Petrographical and petrological features of gneisses in the Pütürge (Malatya) massive*. 20th Year Geology Symposium, May 12–16, 1997, Selçuk University Faculty of Engineering-Architecture, Konya, Proceedings, pp. 217–227 (in Turkish, with English abstract).

Espenshade, G.H. and Potter, D.B. (1960) *Kyanite, sillimanite and andalusite deposits of southeastern States*. U.S. Geological Survey Professional Paper, 336 pp.

Evans, B.W. and Guggenheim, S. (1988) Talc, pyrophyllite, and related minerals. Pp. 225–294 in: *Hydrous Phyllosilicates (Exclusive of Micas)* (S.W. Bailey, editor). Reviews in Mineralogy **19**, Mineralogical Society of America, Washington, D.C.

Frey, M. (1987) Very low-grade metamorphism of clastic sedimentary rocks. Pp. 9–58 in: *Low Temperature Metamorphism* (M. Frey, editor), Blackie and Son, Glasgow, UK.

Gençoğlu, H., Bayhan, H. and Yalçın, H. (1989) Mineralogy and genesis of the kaolinite deposits around the Bilecik-Söğüt area. Pp: 97–112 in: *Proceedings of IVth Turkish National Clay Symposium* (D. Boztuğ and H. Yalçın, editors). 20–23 September, Cumhuriyet University, Sivas, Turkey (in Turkish, with English abstract).

Gilg, H.A. and Sheppard, S.M.F. (1996) Hydrogen isotope fractionation between kaolinite and water revisited. *Geochimica et Cosmochimica Acta*, **60**, 529–533.

Göncüoğlu, M.C. (1997) Distribution of Lower Paleozoic rocks in the Alpine terranes of Turkey: Paleogeographic constraints. Pp. 13–23 in: *Early Paleozoic Evolution in NW Gondwana*. Turkish Associations of Petroleum Geologists, Special Publications **3**. Ankara, Turkey.

Gromet, L.P., Dymek, R.F., Haskin, L.A. and Korotev, R.L. (1984) The North American shale composite: Its compilation, major and trace element characteristics. *Geochimica et Cosmochimica Acta*, **48**, 2469–2482.

Haskin, L.A., Haskin, M.A., Frey, F.A. and Wideman, T.R. (1968) Relative and absolute terrestrial abundances of the rare earths. Pp. 880–912 in: *Origin and Distribution of the Elements* (L.H. Ahrens, editor). Pergamon Press, Oxford, UK.

Hemley, J.J., Montoya, J.W., Marinenko, J.W. and Luce, R.W. (1980) Equilibria in the system Al_2O_3-SiO_2-H_2O and some general implications for alteration/mineralization processes. *Economic Geology*, **75**, 210–228.

Hoefs, J. (1984) *Stable Isotope Geochemistry*, 3rd edition. Springer Verlag, Berlin, 241 pp.

J.C.P.D.S. (1990) Powder Diffraction File: Alphabetical Indexes Inorganic Phases. Swarthmore, USA, 871 pp.

Kawakami, T. and Ikeda, T. (2003) Boron in metapelites controlled by the breakdown of tourmaline and retrograde formation of borosilicates in the Yanai area, Ryoke metamorphic belt, SW Japan. *Contributions to Mineralogy and Petrology*, **145**, 131–150.

Keller, W.D. (1976) Scan electron micrographs of kaolins collected from diverse environments of origin-I. *Clays and Clay Minerals*, **24**, 107–113.

Keller, W.D. (1978) Classification of kaolins exemplified by their textures in scan electron micrographs. *Clays and Clay Minerals*, **26**, 1–20.

Kontak, D.J., Finck, P.W. and De Wolfe, J. (2004) *Pyrophyllite occurrences in the Coxheath area, Cape Breton Island*. Natural Resources Branch, Nova Scotia, Report ME-2004-1, pp. 1–18.

Kutbay, C. (1998) Pyrophyllite, the rare jewel of tile manufacturing. *Ceramic Industry*, October, pp. 43–45.

Marumo, K. (1989) Genesis of kaolin minerals and pyrophyllite in Kuroko deposits of Japan. Implications for the origins of the hydrothermal fluids from mineralogical and stable isotope data. *Geochimica et Cosmochimica Acta*, **53**, 2915–2924.

Merriman, R.J. and Peacor, D.R. (1999) Very low-grade metapelites: mineralogy, microfabrics and measuring reaction progress. Pp. 10–60 in: *Low-Grade Metamorphism* (M. Frey and D. Robinson, editors), Blackwell, Oxford, UK.

Murray, H.H. (1988) Kaolin minerals: Their genesis and occurrences. Pp. 67–89 in: *Hydrous Phyllosilicates (Exclusive of Micas)* (S.W. Bailey, editor). Reviews in Mineralogy **19**, Mineralogical Society of America, Washington, D.C.

Nabetani, A. and Shikazono, N. (2002) Chemical process and environment of hydrothermal alteration of acidic volcanic rocks in the Mitsuishi district, southwest Japan. *Geochemical Journal*, **36**, 255–269.

Önal, A. and Bingöl, A.F. (1997) Geology of western part of Doğanşehir (Malatya, Turkey). *Selçuk University Journal of the Faculty of Engineering-Architecture*, **12**, 63–75 (in Turkish, with English abstract).

Ruiz-Cruz, M.D. and Reyes, E. (1998) Kaolinite and dickite formation during shale diagenesis. Isotopic data. *Applied Geochemistry*, **13**, 95–104.

Şengör, A.M.C. and Yılmaz, Y. (1981) Tethyan evolution of Turkey: A plate tectonic approach. *Tectonophysics*, **75**, 181–241.

Sheppard, S.M.F. (1986) Characterization and isotopic variations in natural waters. Pp. 165–184 in: *Stable Isotopes in High-temperature Geological Processes* (J.W. Valley, Jr., H.P. Taylor and J. O'Neil, editors). Reviews in Mineralogy **16**, Mineralogical Society of America, Washington D.C.

Sheppard, S.M.F. and Gilg, H.A. (1996) Stable isotope geochemistry of clay minerals. *Clay Minerals*, **31**, 1–24.

Sheppard, S.M.F., Nielsen, R.L. and Taylor, H.P. Jr. (1969) Oxygen and hydrogen isotope ratios of clay minerals from porphyry copper deposits. *Economic Geology*, **64**, 755–777.

Shepherd, T.J., Rankin, A.H. and Alderton, D.H.M. (1985) *A Practical Guide to Fluid Inclusion Studies*. Blackie, Glasgow, UK, 235 pp.

Sudo, T., Shimoda, S., Yotsumoto, H. and Aita, S. (1981) *Electron Micrographs of Clay Minerals*. Developments in Sedimentology **31**, Elsevier, Tokyo, 203 pp.

Sun, S.S. and McDonough, W.F. (1989) Chemical and isotopic systematics of ocean basalts. Implications for mantle composition and processes. Pp. 313–345 in: *Magmatism in Ocean Basins* (A.F. Saunders, M.J. Norry, editors), Special Publication **42**, Geological Society, London.

Sykes, M.L. and Moody, J.B. (1978) Pyrophyllite and

metamorphism in the Carolina slate belt. *American Mineralogist*, **63**, 96–108.

Telek, E. (1979) *Study report of MTA-licensed pyrophyllite fields in Malatya-Pütürge*. General Directorate of Mineral Research and Exploration, Directorate of Malatya Region, Project No. 263, 15 pp.

Terakado, Y. and Fujitani, T. (1998) Behavior of the rare earth elements and other trace elements during interactions between acidic hydrothermal solutions and silicic volcanic rocks, southwestern Japan. *Geochimica et Cosmochimica Acta*, **62**, 1903–1917.

Turan, M., Aksoy, E. and Bingöl, A.F. (1995) Characteristics of the geodynamic evolution of eastern Taurus in Elazığ region (E. Turkey). *Fırat University Bulletin of the Science and Engineering*, **7**, 177–199 (in Turkish, with English abstract).

Urabe, T. (1987) Kuroko deposits modeling based on magmatic hydrothermal theory. *Mining Geology*, **37**, 159–176.

Uygun, A. and Solakoğlu, E. (2002) Geology and origin of pyrophyllite deposits in the Pütürge (Malatya) massive. *Bulletin of the Mineral Research and Exploration*, **123**/**124**, 13–19 (in Turkish).

Veniale, F., Delgado, A., Marinoni, L. and Setti, M. (2002) Dickite genesis in the 'varicoloured' clay-shale formation of the Italian Apennines: an isotopic approach. *Clay Minerals*, **37**, 255–266.

Yalçın, H. (1991) Morphology and chemistry of hydrothermal kaolinites: Examples from Eskişehir and Malatya province. Pp. 74–86 in: *Proceedings of Vth Turkish National Clay Symposium* (M. Zor, editor). 16–20 September, Anadolu University, Eskişehir, Turkey (in Turkish, with English abstract).

Yalçın, H. and Bozkaya, Ö. (2003) Mineralogy and geochemistry of hydrothermal kaolinite and I-S occurrences, (Yıldızeli-Akdağmadeni) W-Sivas. *Geological Bulletin of Turkey*, **46**, 1–23 (in Turkish, with English abstract).

Yazgan, E. (1981) A study of active continental paleomargin in the eastern Taurides (Upper Cretaceous-Middle Eocene), Malatya-Elazığ (Eastern Turkey). *Bulletin of the Institute of Earth Sciences of Hacettepe University*, **7**, 83–104 (in Turkish, with English abstract).

Yazgan, E. and Chessex, R. (1991) Geology and tectonic evolution of the southeastern Taurides in the region of Malatya. *Bulletin of the Turkish Association of Petroleum Geologists*, **3**, 1–42.

Yazgan, E., Michard, A., Whitechurch, H. and Montigny, R. (1983) Le Taurus de Malatya (Turquie orientale) élément de la suture sud-téthysienne. *Bulletin de la Sociéte Geologique de France*, **25**, 59–69.

Yılmaz, Y. (1993) New evidence and model on the evolution of the southeast Anatolian orogen. *Geological Society of America Bulletin*, **105**, 251–271.

Yılmaz, H., Aras, A. and Ağrılı, H. (1993) *The mining geology of Taşmış–Pütürge (Malatya) pyrophyllite deposits*. General Directorate of Mineral Research and Exploration, Project No. 9598, 22 p (in Turkish).

Yiğitbaş, E. and Yılmaz, Y. (1996) New evidence and solution to the Maden complex controversy of the southeast Anatolian orogenic belt (Turkey). *Geologische Rundschau*, **85**, 250–263.

Zen, E.A.N. and Albee, A.L. (1964) Coexistent muscovite and paragonite in pelitic schists. *American Mineralogist*, **49**, 904–925.

Zheng, Y.-F. (1993a) Calculation of oxygen isotope fractionation in anhydrous silicate minerals. *Geochimica et Cosmochimica Acta*, **57**, 1079–1091.

Zheng, Y.-F. (1993b) Calculation of oxygen isotope fractionation in hydroxyl-bearing silicates. *Earth and Planetary Science Letters*, **120**, 247–263.

(*Received 9 October 2006; revised 18 April 2007; Ms. 1224; A.E. W. Crawford Elliott*)